Published OnlineFirst September 3, 2019; DOI: 10.1158/1078-0432.CCR-19-0976

Translational Cancer Mechanisms and Therapy

Clinical Cancer Research

Combination of PPARγ Agonist Pioglitazone and Trabectedin Induce Adipocyte Differentiation to Overcome Trabectedin Resistance in Myxoid Liposarcomas

Roberta Frapolli[1], Ezia Bello[1], Marianna Ponzo[1], Ilaria Craparotta[2], Laura Mannarino[2], Sara Ballabio[2], Sergio Marchini[2], Laura Carrassa[3], Paolo Ubezio[4], Luca Porcu[5], Silvia Brich[6], Roberta Sanfilippo[7], Paolo Giovanni Casali[7], Alessandro Gronchi[8], Silvana Pilotti[6], and Maurizio D'Incalci[9]

Abstract

Purpose: This study was aimed at investigating whether the PPARγ agonist pioglitazone—given in combination with trabectedin—is able to reactivate adipocytic differentiation in myxoid liposarcoma (MLS) patient-derived xenografts, overcoming resistance to trabectedin.

Experimental Design: The antitumor and biological effects of trabectedin, pioglitazone, and the combination of the two drugs were investigated in nude mice bearing well-characterized MLS xenografts representative of innate or acquired resistance against trabectedin. Pioglitazone and trabectedin were given by daily oral and weekly i.v. administrations, respectively. Molecular studies were performed by using microarrays approach, real-time PCR, and Western blotting.

Results: We found that the resistance of MLS against trabectedin is associated with the lack of activation of adipogenesis. The PPARγ agonist pioglitazone reactivated adipogenesis, assessed by histologic and gene pathway analyses. Pioglitazone was well tolerated and did not increase the toxicity of trabectedin. The ability of pioglitazone to reactivate adipocytic differentiation was observed by morphologic examination, and it is consistent with the increased expression of genes such as *ADIPOQ* implicated in the adipogenesis process. The determination of adiponectin by Western blotting constitutes a good and reliable biomarker related to MLS adipocytic differentiation.

Conclusions: The finding that the combination of pioglitazone and trabectedin induces terminal adipocytic differentiation of some MLSs with the complete pathologic response and cure of tumor-bearing mice provides a strong rationale to test the combination of trabectedin and pioglitazone in patients with MLS.

Introduction

Trabectedin is a marine alkaloid originally extracted from a Caribbean tunicate and now prepared synthetically. It binds the minor groove of DNA, causing a distortion of the double helix that bends toward the major groove. Part of the molecule protrudes from the DNA interacting with DNA binding proteins. Trabectedin interacts with DNA-repair pathways and directly affects trans-activated transcription. It also modulates cytokine and chemokine production by cancer cells and tumor-associated macrophages. Due to these unique mechanisms of action, trabectedin acts against both tumor cells and the tumor microenvironment (1–3). In 2007, the drug was approved by the European Medicines Agency (EMA) for the treatment of adult patients with advanced soft-tissue sarcomas (STS) after the failure of anthracyclines and ifosfamide or for patients who cannot be given these medicines (4). In 2015, trabectedin also received FDA approval for the treatment of patients with unresectable or metastatic liposarcoma and leyomiosarcoma who received a prior anthracycline-containing regimen (5). Within the different histologic subtypes of STS, leyomiosarcomas and liposarcomas seem to benefit more than other subtypes from treatment with trabectedin. In particular, in myxoid liposarcomas (MLS)—an STS histotype generally associated with a good chemosensitivity—trabectedin has shown a very good activity. A retrospective study

[1]Unit of Preclinical Experimental Therapeutics, Department of Oncology, Istituto di Ricerche Farmacologiche Mario Negri IRCCS, Milan, Italy. [2]Unit of Translational Genomic, Department of Oncology, Istituto di Ricerche Farmacologiche Mario Negri IRCCS, Milan, Italy. [3]Unit of DNA repair, Department of Oncology, Istituto di Ricerche Farmacologiche Mario Negri IRCCS, Milan, Italy. [4]Unit of Biophysics, Department of Oncology, Istituto di Ricerche Farmacologiche Mario Negri IRCCS, Milan, Italy. [5]Unit of Methodological Research, Department of Oncology, Istituto di Ricerche Farmacologiche Mario Negri IRCCS, Milan, Italy. [6]Laboratory of Molecular Pathology, Department of Pathology, Fondazione IRCCS Istituto Nazionale dei Tumori, Milan, Italy. [7]Medical Oncology Unit 2, Fondazione IRCCS Istituto Nazionale dei Tumori, Milan, Italy. [8]Department of Surgery, Fondazione IRCCS Istituto Nazionale dei Tumori, Milan, Italy. [9]Department of Oncology, Istituto di Ricerche Farmacologiche Mario Negri IRCCS, Milan, Italy.

Note: Supplementary data for this article are available at Clinical Cancer Research Online (http://clincancerres.aacrjournals.org/).

Corrected online January 15, 2020.

Corresponding Author: Maurizio D'Incalci, Instituto di Ricerche Farmacologiche Mario Negri—IRCCS, via La Masa 19, 20156 Milan, Italy. Phone: 39-02-3901-4571; Fax: 39-02-3901-4734; E-mail: maurizio.dincalci@marionegri.it

Clin Cancer Res 2020;25:7565–75

doi: 10.1158/1078-0432.CCR-19-0976

Published OnlineFirst September 3, 2019; DOI: 10.1158/1078-0432.CCR-19-0976

Translational Relevance

Although trabectedin is a very effective drug for the treatment of metastatic myxoid liposarcomas (MLS), with approximately 80% response rate, there are cases that are resistant to the drug. Furthermore, most patients who respond—response generally lasts several months—acquire resistance and eventually die of disease progression. In MLS xenografts, the combination of the PPARγ agonist pioglitazone with trabectedin was more effective than trabectedin alone in inducing adipocytic differentiation. The combination caused long-lasting pathologic responses even in MLS xenografts that were resistant against trabectedin. Terminal differentiation accompanied curative effects in some tumors. The antitumor activity, consistency of the morphologic and molecular data, and lack of toxicity of pioglitazone provide a strong rationale to test the combination in a clinical trial.

enrolling 51 pretreated MLS patients reported two complete responses and 24 partial responses, with an overall responses rate of 51% and a progression-free survival at 6 months of 88%. In most of the responding patients, changes in tissue density were observed during the radiologic evaluations before tumor shrinkage. Histologic analysis conducted after trabectedin treatment on surgically resected tumors showed major pathologic responses characterized by cellular depletion, disappearance of the vascular network, deposition of myxoid stroma, and appearance of monovacuolated adipoblasts (6). Further studies confirmed the exquisite sensitivity of MLS to trabectedin even in the neoadjuvant setting (7–9). Unlike anthracyclines, trabectedin has a good toxicity profile and does not cause cumulative toxicity, allowing prolonged treatment that lasts until tumor progression (10). At this stage, effective therapeutic options are not available for trabectedin-resistant MLS patients.

From a molecular point of view, MLS is characterized by the chromosomal translocation t(12;16) (q13;p11), resulting in the *FUS–CHOP* fusion gene. Rarely, the translocation t(12;22)(q13;q12) occurs, giving rise to the EWS–CHOP chimera. These translocations are recognized as being the pathogenic event that leads to MLS development (11–15). The aberrant transcription factor represses the expression of the master regulator of adipogenesis, PPARγ-2 and cEBPα, thus causing the inhibition of the late stages of adipogenesis (16, 17) with the accumulation of immature adipoblasts that proliferate without undergoing terminal differentiation.

The unusual mechanism of action of trabectedin in MLS was investigated in a panel of patient-derived xenografts (PDXs; refs. 18, 19). In these preclinical models as well as in a human biopsy, trabectedin was able to displace the protein FUS–CHOP from the promoters of its target genes. The inactivation of the chimera allows the reactivation of adipogenesis with consequent differentiation of adipocytes (19). The ability of trabectedin to detach FUS–CHOP from DNA appeared to be reduced in PDX models of MLS that are resistant to trabectedin treatment and do not undergo adipocyte maturation (19, 20).

A central role in adipogenesis is carried out by the peroxisome proliferator-activated receptor gamma (PPARγ). PPARγ activates the expression of cEBPα and vice versa in a positive loop. PPARγ and cEBPα cooperate in the regulation of the expression of several genes involved in adipocytic maturation (21). Thiazolidendiones are a class of antidiabetic drugs that act as PPARγ agonists. They have shown anticancer properties in several preclinical models, both *in vitro* and *in vivo*, where cell-cycle arrest, inhibition of angiogenesis, and differentiation and apoptosis were observed (22–26). In the clinic, no or very few responses were observed in phase II trials with this class of compounds in solid tumors (27–29). Nevertheless, Demetri and colleagues described dramatic tissue responses, with lipid accumulation in the cell cytoplasm and reduction of the proliferation marker Ki-67 in two cases of MLS and one pleomorphic liposarcoma patient, who received the PPARγ agonist troglitazone (30). A subsequent phase I study conducted with efatutazone in patients with advanced solid malignancies showed a prolonged partial response in a patient with metastatic MLS (31). These data suggest that PPARγ agonists can overcome the block of adipocyte differentiation induced by the fusion protein.

The possibility of combining trabectedin with PPARγ agonists was first hypothesized by Charytonowicz and colleagues (32). In a transgenic mouse model of MLS that was sensitive to trabectedin, they observed that rosiglitazone enhanced trabectedin-induced adipogenesis with a considerable improvement in mouse survival.

In this work, we tested the combination of trabectedin with the PPARγ agonist pioglitazone in various MLS PDXs characterized by different sensitivity to trabectedin. The efficacy results together with the obtained pathologic and molecular data provide a strong rationale for the clinical development of this combination.

Materials and Methods

Animals

Six- to 8-week-old female Athymic nude mice were obtained from Envigo. Animals were housed and handled under specific pathogen-free conditions in the Institute's Animal Care Facilities, which meet international standards; they are regularly checked by a certified veterinarian who is responsible for health monitoring, animal welfare supervision, experimental protocols and procedures revision.

Procedures involving animals and their care were conducted in conformity with the following laws, regulations, and policies governing the care and use of laboratory animals: Italian Governing Law (D.lgs 26/2014; Authorization n.19/2008-A issued March 6, 2008, by the Ministry of Health); Mario Negri Institutional Regulations and Policies providing internal authorization for persons conducting animal experiments (Quality Management System Certificate—UNI EN ISO 9001:2008—Reg. No. 6121); the NIH Guide for the Care and Use of Laboratory Animals (2011 edition) and EU directives and guidelines (EEC Council Directive 2010/63/UE), and in line with guidelines for the welfare and use of animals in cancer research (33).

Experimental protocols have been reviewed and approved by the IRFMN Animal Care and Use Committee, which includes members "*ad hoc*" for ethical issues, and by the Italian Ministry of Health.

Drugs

Trabectedin (Yondelis) was provided by PharmaMar, S.A.; it was dissolved in water and further diluted in saline immediately before use.

Published OnlineFirst September 3, 2019; DOI: 10.1158/1078-0432.CCR-19-0976

Pioglitazone (Takeda) was dissolved in 10% DMSO and diluted with methocell 0.5% added with Tween 80 0.5%.

Tumor models

ML006 and ML017 patient–derived MLS xenografts were obtained from biopsies of patients suffering from round cell (RC) variant of MLS and maintained through serial transplantation in mice as previously described (18). ML006 was characterized by an innate resistance to trabectedin, whereas ML017 was very sensitive. ML017/ET was obtained from ML017 through exposition at repeated *in vivo* cycles of trabectedin acquiring a resistant phenotype (20). The histologic features of the tumors grown in mice were verified after each passage, and compared with that of the original human sample in order to maintain the clinical relevance of these models.

In vivo study

When tumor burden reached about 300 to 400 mg, mice bearing ML006, ML017, or ML017/ET xenografts were randomized to receive trabectedin 0.15 mg/kg i.v., every 7 days for three times (q7d×3), pioglitazone 150 mg/kg p.o. daily for 28 days or their combination. Tumor growth was measured using Vernier caliper, and tumor weights were calculated by the formula: length $\times$ $(\text{width})^2/2$.

To perform molecular and pathologic studies, tumor-bearing mice were treated as described above. Fourteen days after the last dose of trabectedin (3 hours after the last dose of pioglitazone), mice were sacrificed. Tumor samples were collected, frozen in dry ice or formalin-fixed and paraffin-embedded for hematoxylin/eosin staining. At least three biological replicates were used for each experimental condition.

Analysis of the tumor growth curves

Each tumor weight (TW) measure was normalized to the tumor weight of the same mouse at the start of treatment, and treatment efficacy was evaluated in the normalized tumor weight curve of individual mice using three independent parameters: tumor growth (usually referred to as "growth inhibition," GI) during treatment, tumor weight at nadir (TW_{nadir}), and absolute growth delay (AGD).

The percentage of GI, indicative of the short-term antiproliferative effect, measures the relative tumor growth between the start (day 0) and the end (day X) of treatment and was calculated adapting the NCI definition (33, 34) to the case:

$\%GI_{0\text{-}X} = [(TWT_X - TWT_0)/(\langle TWC_X\rangle - \langle TWC_0\rangle)] \times 100$ when $TWT_X \geq \langle TWC_0\rangle$;

$\%GI_{0\text{-}X} = [(TWT_X - TWT_0)/\langle TWC_0\rangle] \times 100$ when $TWT_X < \langle TWC_0\rangle$,

where $(TWT_X - TWT_0)$ is the increment of the tumor weight between day 0 and day X of the treated (T) tumor under analysis, $(\langle TWC_X\rangle - \langle TWC_0\rangle)$ is the same increment as averages in the control (C) group (both TWT_0 and $\langle TWC_0\rangle$ are equal 1 by effect of the previous normalization).

TW_{nadir}, indicative of the extent of tumor shrinkage (usually in the middle-term after treatment), is the minimum reached by the normalized tumor growth curve, from the start of treatment. In controls and when no tumor regression was observed, TW_{nadir} was equal to 1 (the normalized weight at the start of treatment).

AGD, indicative of the long-term delay of tumor regrowth, was calculated as the difference (in days) between the time to reach a target size in a treated tumor and the median time to reach the same size in the control group (35, 36). Depending on tumor growth curves, AGD was calculated at four or six times the size at the start of treatment (AGD4 and AGD6, respectively).

Histologic characterization

The histologic criteria applied to define MLS histotype and its usual and RC subtypes were the ones described in the WHO classification (38).

Microarray experiment and data quantification

RNA was extracted using the miRNeasy Mini kit (QIAGEN), according to the manufacturer's protocols. Using the Low Input Quick Amp Labeling Kit (Agilent Technologies), 150 ng of total RNA was reverse transcribed into Cy3-labeled cRNA and then hybridized onto commercially available array platforms as previously described (39). For each treatment, at least three biological or technical replicates were used. Raw data from Agilent Feature Extraction version 11 were preprocessed, removing features marked as unreliable by the scanning software. Arrays were normalized using the "quantile" method (40), and a batch correction was applied to normalized data. Raw data are available on the ArrayExpress database, under accession ID E-MTAB-8632.

Differential expression analysis

A linear model for microarray analysis (41) was used to determine differentially expressed genes applying a correction for technical replicates and for batch bias (42) and setting a log fold-change cutoff at ± 1, and false discovery rate corrected *P* value less than or equal to 0.05 (43). Each comparison was performed setting treated samples versus untreated control.

Functional enrichment analysis

Gene Set Enrichment Analysis (44) was used for functional enrichment analysis comparing gene-expression data from each treatment with untreated controls, using default parameters. Gene sets used were biological states or processes defined as hallmark (50 gene sets; ref. 45) and Biological Process from the Gene Ontology (46), both retrieved from the Molecular Signature Database (MSigDB, version 6.1). EnrichmentMap application version 3.0.0 of Cytoscape version 3.6.0 was used for plotting, setting a $P < 0.01$, q-value <0.05, and using the overlap parameter set at 0.20.

Real-time PCR

Total RNA (250 ng) was reverse transcribed using the High-Capacity cDNA Reverse Transcription Kit according to the manufacturer's instructions (Applied Biosystems). Real-time PCR was performed in triplicate for each case by using specific primer for five selected genes (belonging to the adipogenesis pathway) found to be differentially expressed in treated tissue samples compared with untreated control. These genes were *LIPE*, *ADIPOQ*, *LPL*, *FABP4*, and *PLIN1*. All the reactions were carried out on the 7900HT Fast Real-Time PCR System (Applied Biosystems) using QuantiFast SYBR Green PCR Master Mix (Qiagen). Data were normalized using geometric mean of two selected invariant genes (*CARNMT1* and *G6PD*). Analysis was performed by using the $2^{-\Delta\Delta Ct}$ protocol and expressed as fluorescence intensity arbitrary unit.

Western blotting analysis

Proteins, extracted from the frozen specimens, were homogenized in protein lysis buffer, loaded on SDS-PAGE and

Published OnlineFirst September 3, 2019; DOI: 10.1158/1078-0432.CCR-19-0976

immunoblotted as previously described (44, 47). Odissey FC Imaging System (LI-COR) was used for the acquisition. Primary antiadiponectin (1:1,000, cat. No. ab22554) was purchased from Abcam, and actin (1:500, cat. No. sc-1616) was purchased from Santa Cruz Biotechnology.

Statistical methods

Treatment effect on xenograft tumor growth curves has been formally tested using a nonparametric approach. For each mouse, the partial tumor growth rates (k) between every time interval were calculated as follows: $k = [\log(TW_{ti+1}) - \log(TW_{ti})]/(t_{i+1} - t_i)$. The experimental groups were compared two by two using a Wilcoxon rank-sum test, stratified by time intervals, on the obtained k values.

The Student *t* test for unpaired samples was used to compare %GI, TW_{nadir}, and AGD parameters and real-time PCR data between different treatment groups.

Results

The antitumor efficacy of trabectedin in combination with pioglitazone was studied in three PDX models of RC MLS characterized by different sensitivities to trabectedin. ML017 is very sensitive, whereas ML006 shows an innate partial resistance to the drug. ML017/ET was obtained from ML017 through the administration of 10 cycles of trabectedin *in vivo*. Once obtained, the resistant phenotype was stable, being maintained for several passages in mice without further treatment. Tumor growth curves are shown in Fig. 1. In all xenograft models, the combination of trabectedin with pioglitazone significantly improved tumor response compared with single-agent treatments ($P < 0.001$ in ML006, $P < 0.05$ in ML017, and $P < 0.01$ in ML017/ET).

A more in-depth analysis of the response to treatment was made considering short, intermediate, and long-term characteristics of the tumor volume versus time curve for each individual tumor. A score of the short-term response to treatment was obtained based on the growth inhibition measured on the increase/decrease of tumor volume at the end of treatment (or alternatively on the day of sacrifice because of ethically acceptable endpoint, that is, TW $\geq$ 1.5 g had been reached), compared with the volume at the start of treatment ($\%GI_{0\text{-}X}$). The intermediate-time score was provided by the minimum value of the tumor weight (TW_{nadir}) relative to the weight at treatment start (TW_0). Absolute growth delay (AGD4) was calculated by the time to reach a target relative volume (4 times the size at the start of treatment) minus the median time to reach the same target in the control group.

As shown in Fig. 1A, the growth of untreated ML006 tumors was very slow, with doubling times of Td = 37.8 ± 5.0 days (N = 10 tumors). In this model, trabectedin and the combination with pioglitazone induced a strong GI, while a modest GI was detected in the pioglitazone alone group.

Some variability was observed in the group of mice treated with trabectedin alone: after initial growth inhibition during treatment (average %GI = 32%), prolonged tumor growth arrest was achieved in four of 10 tumors, while the others regrew with 52 days' average AGD4.

A closer inspection of the time course of TW indicates that pioglitazone alone progressively reduced the tumor growth rate with complete arrest in week 3. The pioglitazone-induced growth arrest, without shrinkage, continued for a long time after treatment discontinuation, up to the end of follow-up (6 months) in four of 10 ML006 tumors. The other tumors eventually regrew, with 55 days' average AGD4.

The combination enabled us to consolidate the response achieving robust (>40%) tumor shrinkage in seven of nine tumors and minor shrinkage in two, with 0.39 average TW_{nadir}. Complete responses were achieved in three of nine tumors with undetectable residual mass at sacrifice, and partial responses in four of nine mice, with tumor size remaining unchanged from the end of treatment. A very slow regrowth (98 days AGD4) was observed in only one tumor. One mouse died for undiagnosed reasons 1 week after the last trabectedin dose, its body weight loss was ~10%.

ML017 tumors were characterized by a doubling time of 10.9 ± 3.3 days (N = 15), shorter than that of the ML006 tumor. As a consequence, untreated tumors reached maximal size within 3 weeks, and mice had to be killed for ethical reasons (Fig. 1B). Trabectedin-induced growth inhibition was already observed in the first week of treatment and tumor shrinkage occurred in the second, leading to a negative %GI on day 13. Tumor shrinkage continued during trabectedin treatment and for some days after its discontinuation, reaching a nadir ($TW_{nadir} = 0.58 \pm 0.06$) on day 30 (median value). Thereafter, all tumors regrew, with an average AGD4 of 46 days. Pioglitazone alone did not inhibit tumor growth. Tumors in pioglitazone-treated animals grew even faster than controls, and mice were sacrificed on day 13. This rapid growth might have prevented the observation of a posttreatment inhibition, as observed in the ML006 model. The effects of the treatment combination were significantly superior to those of trabectedin alone, reaching a very low nadir ($TW_{nadir} = 0.23 \pm 0.03$). The combination delayed regrowth (average AGD4: 69 days), which occurred in two mice only after 4 months.

In mice bearing trabectedin-resistant ML017/ET tumors, tumor growth was faster than in animals with their sensitive counterpart (DT 7.4 ± 0.4 days, N = 11). In these mice, pioglitazone-treated tumors could be measured up to the third week (Fig. 1C), allowing detection of both an initial fast growth phase ($GI_{0\text{-}7} = 163\%$) and a subsequent decreased growth rate in week 3 ($GI_{0\text{-}21} = 91\%$). As expected, trabectedin was much less effective in these mice than in the ML017 tumor–bearing mice without observable tumor growth arrest or shrinkage. AGD6 was only 12 days on average.

In mice bearing the ML017/ET tumor, the combination was more efficacious than trabectedin alone with values of 35% $GI_{0\text{-}21}$ and 23 days AGD6. Tumor regression was not observed, and all tumors regrew in the fifth week. Nevertheless, the addition of pioglitazone to the treatment regimen caused a reduction in growth rate (Td = 16.7 ± 1.1 days, range, 12–24 days). This in turn caused prolongation in murine survival, i.e., the period within which maximal TW was achieved (1.5–2 g), by about 20 days compared with mice treated with trabectedin only.

The efficacy of the combined treatment was further confirmed in the ML004 model, another PDX partially resistant to trabectedin (Supplementary Fig. S1). Both trabectedin and pioglitazone were well tolerated with minimal or no body weight loss and absence of clinical signs of distress. Likewise, the combination did not increase toxicity (Fig. 2A–C).

Morphologically, in samples from all three xenografts from untreated mice, the observed pattern of growth was consistent with the RC variant of MLS. However, ML006 tumors presented with more intervening stroma than ML017 and ML017/ET tumors, consistent with the differences in doubling times. ML006 tumors in mice that received trabectedin showed a decrease of

Published OnlineFirst September 3, 2019; DOI: 10.1158/1078-0432.CCR-19-0976

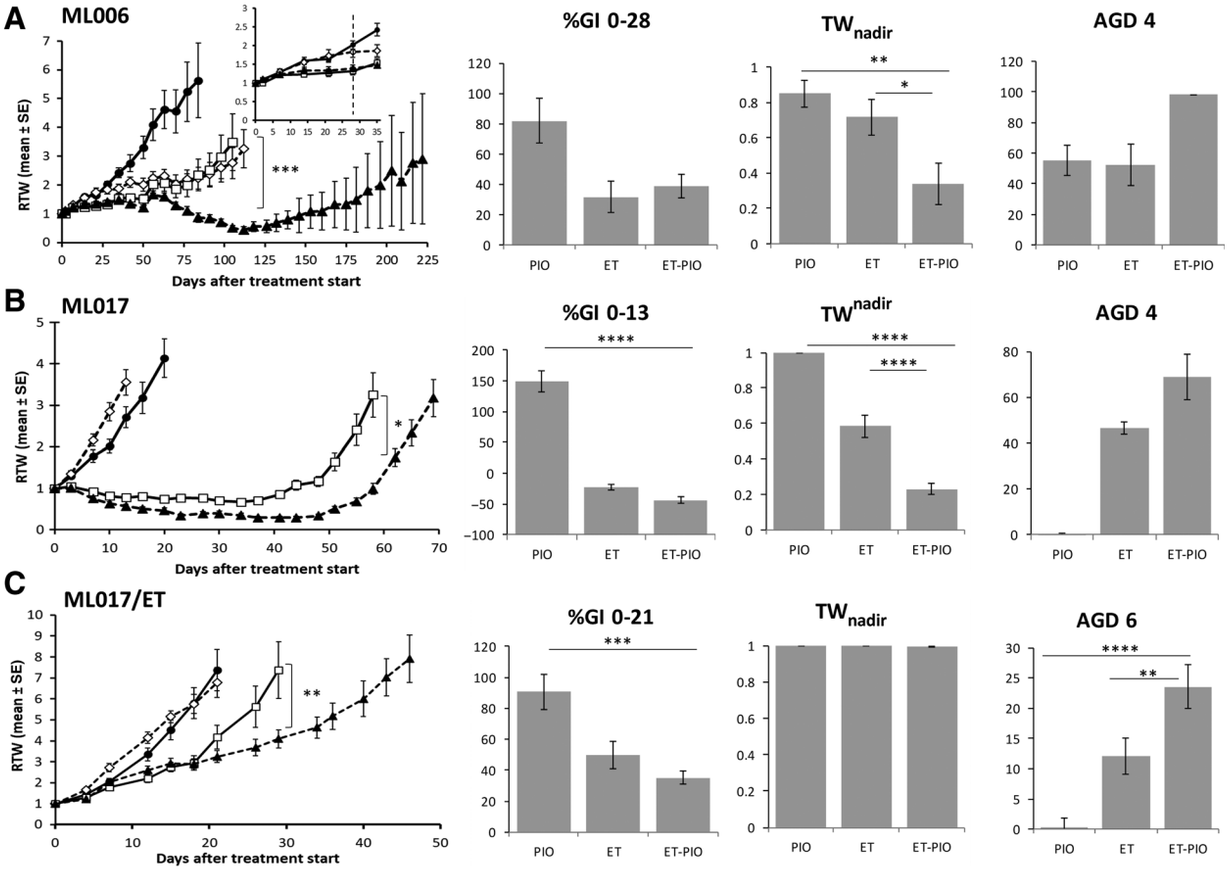

Figure 1.

Antitumor activity of trabectedin, pioglitazone and their combination in MLS PDX. Relative TW in ML006 (**A**), ML017 (**B**), and ML017/ET (**C**) xenografts: tumor-bearing mice were treated with saline (●) trabectedin (ET) 0.15 mg/kg i.v., q7dx3 (□), pioglitazone (PIO) 150 mg/kg qd×28 (◇) or their combination (ET-PIO▲). Treatment started when the mean TW was about 250 to 350 mg. The time course of the response to treatment was measured by three independent parameters indicative of (i) early antiproliferative effects (tumor growth during treatment, %GI); (ii) tumor shrinkage (if any; tumor weight at nadir, TW_{nadir}); (iii) time delay before regrowth (absolute growth delay, AGD). The calculation was made for each single mouse and values are reported as mean ± SD. Statistical analysis: *, $P < 0.05$; **, $P < 0.01$; ***, $P < 0.001$; ****, $P < 0.0001$.

cellularity and vascular supply, in line with the known effect of the drug, but did not show a clear evidence of adipocytic differentiation (Fig. 3A). Adipocytic differentiation, mainly represented by univacuolated lipoblasts harboring hyperchromatic scalloped nuclei, was evident after administration of pioglitazone alone or in combination. Maturation effects persisted and increased after drug discontinuation as visible in a tumor that had regressed for a long time. These observations closely paralleled tumor shrinkage. In mice that received trabectedin, ML017 tumors exhibited a decrease of cellularity with persistence of vascular network, evidence of lipoblastoma-like adipocytic maturation, and occasional white foci of myxoid material in the background (Fig. 3B). All of these findings are consistent with the prolonged growth arrest observed. Pioglitazone administration induced a diffuse microvesicular lipid accumulation without subsequent changes in nuclear morphology. Inconsistent with the observation in ML006 tumors, the nuclei of ML017 tumor cells retained their primitive mesenchymal-like morphology and the maturation effects are not associated with a tumor growth arrest. The combined treatment showed mixed changes, including some effects on the tumor vasculature (Supplementary Fig. S2) that correlated with drug activity eventually leading to delayed tumor regrowth (Fig. 3B).

In mice bearing ML017/ET tumors, trabectedin treatment did not cause morphologic changes when compared with controls, consistent with the lack of tumor growth arrest. After pioglitazone, the immature nonlipogenic RCs showed evidence of lipid accumulation similar to that observed in ML017 tumors. In addition, they exhibited a zonal pattern enriched with signet ring cells. This cell pattern was more prevalent in mice on the combination treatment, consistent with the prolonged AGD (Fig. 3C).

Figure 4 shows a selection of significant pathways engaged by the treatments. As shown in Fig. 4A, in ML006 tumors trabectedin did not activate adipogenic processes, while pioglitazone regulated the adipogenic pathway together with processes related to it, such as fatty acid metabolism and lipid storage. The treatment combination induced adipogenic differentiation, probably due to the preponderance of the effect of pioglitazone. The molecular data are consistent with the H&E staining (Fig. 3A).

Figure 4B and C show the results of the gene-expression array analysis, illustrating networks related to ML017 and ML017/ET tumors: trabectedin alone activated apoptosis, adipogenesis, and

Published OnlineFirst September 3, 2019; DOI: 10.1158/1078-0432.CCR-19-0976

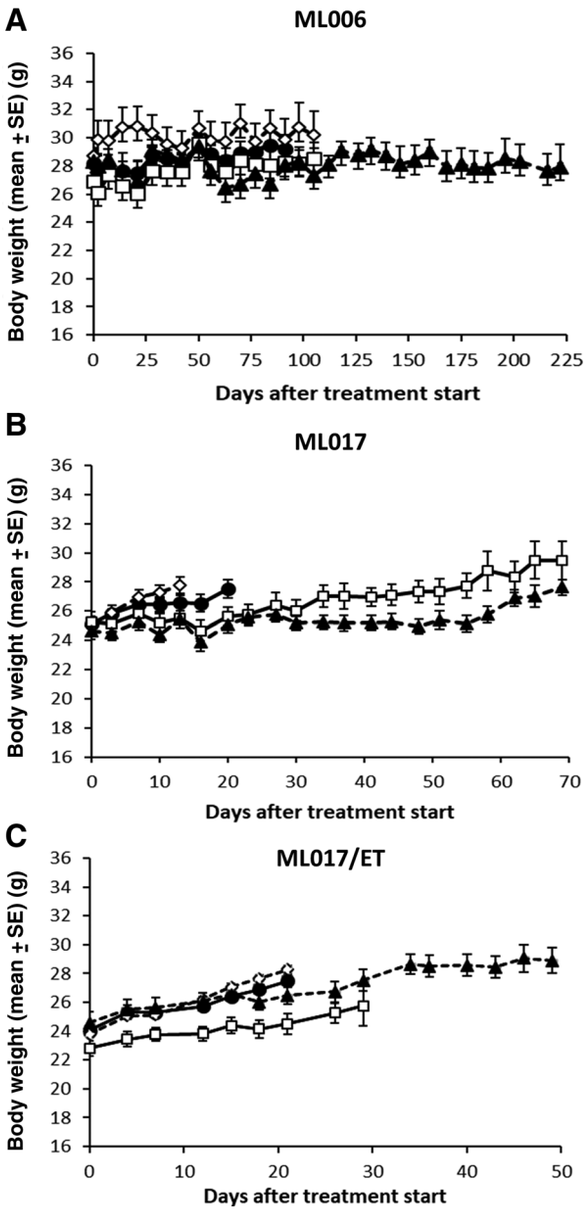

Figure 2.

Treatment tolerability. Body weight in ML006 (**A**), ML017 (**B**), and ML017/ET (**C**) xenografts: tumor-bearing mice were treated with saline (●) trabectedin 0.15 mg/kg i.v., q7d×3 (□), pioglitazone 150 mg/kg qd×28 (◇), or their combination (▲).

several related pathways in the ML017 tumor, while apoptosis and adipogenesis were not significantly modulated in the resistant counterpart. However, processes related to adipogenesis such as lipid storage and positive regulation of lipid transport were seen in ML017/ET tumors. These data are consistent with the morphologic observations (Fig. 3B and C). Pioglitazone alone and in combination activated adipocytic differentiation in both tumor types.

The heat map in Supplementary Fig. S3 shows the levels of expression of major genes implicated in adipogenesis, such as *PPARγ*, *CEBPα*, *FABP4*, *PLIN1*, *LEP*, *AGPAT2*, *GLUT4*, *LPL*, and *ADIPOQ*. As expected, these genes, especially those regulated downstream in the adipogenic process, had higher expression values where the adipogenesis was significantly activated in the network analysis (Fig. 4). Among the genes, *ADIPOQ* (Adiponectin) seemed to be the one of the most expressed. This finding was validated by real-time PCR (Fig. 5A), and this protein was selected as a marker in Western blot studies. Figure 5B shows adiponectin levels confirming its expression where adipogenesis is activated.

Discussion

In this article, we demonstrate that the resistance against trabectedin of PDX of MLS can be overcome by concomitant treatment with the PPARγ agonist pioglitazone. This effect was demonstrated in MLS models of both innate and acquired resistance, and it is associated with the reactivation of adipocytic differentiation.

The overexpression of CHOP is a typical feature of endoplasmic reticulum stress where it is associated with the negative regulation of genes related to lipid homeostasis such as cEBPα (48, 49). Nevertheless, its overexpression in transgenic mice did not cause tumors, while the expression of FUS–CHOP led to the development of liposarcomas, meaning that the FUS domain of the chimera is required for tumorigenesis (13).

The biochemical role of the FUS–CHOP chimera in preventing adipocytic differentiation was previously described (16, 17). They demonstrated downregulation of PPARγ2 and CEBPα expression in different *in vitro* systems, that is, mouse embryonic fibroblast and human liposarcoma cell lines carrying the chimera. These genes are crucial for terminal adipogenesis. This is particularly the case for PPARγ2, which can activate adipogenesis even in the absence of cEBPα. Our group has previously demonstrated, in a panel of MLS PDX, the ability of trabectedin to interfere with the binding of FUS–CHOP to DNA promoters, thus blocking its transcriptional activity (19, 50) and reactivating the differentiation process leading to the maturation of adipoblasts in adipocytes. Adipocytic differentiation following trabectedin treatment was previously reported both in preclinical systems and in the clinic. In MLS patients, after several courses of trabectedin, structural changes assessed by CT and MRI scanning were reported before tumor shrinkage. Biopsies of residual tumor masses confirmed adipocytic maturation of the neoplastic tissue (6, 32), thus indicating that the striking antitumor activity of trabectedin in MLS is related to the activation of adipocytic differentiation. Consistent with previous preclinical (18) and clinical evidence we have observed adipocytic maturation only in the trabectedin-sensitive models such as ML017. In this model, differentiation is associated with increased expression of cEBPα and with the activation of the adipogenic pathway. In contrast, according to both pathologic and molecular analyses, differentiation was not observed in the ML006 or ML017/ET tumors, the first of which harbors innate resistance, and the second of which has acquired resistance against trabectedin. These observations further confirm our previous data according to which lipidic maturation and PPARγ2 expression were observed in the trabectedin-sensitive ML017 and ML015 xenografts, but not in the resistant ML004 (19). These data support the hypothesis that the block of adipocytic maturation could be one of the mechanisms underlying the resistance of MLS against

Published OnlineFirst September 3, 2019; DOI: 10.1158/1078-0432.CCR-19-0976

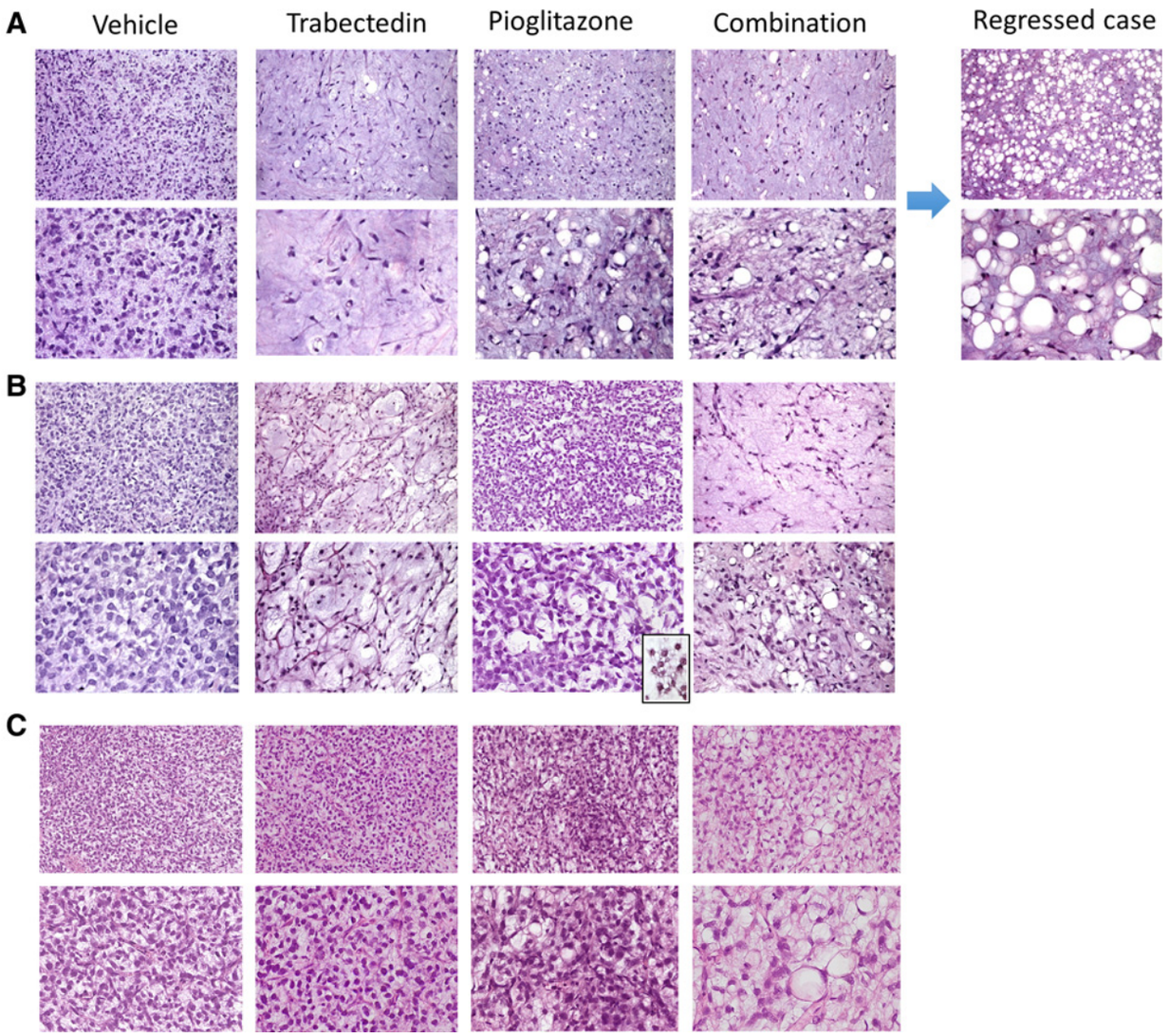

Figure 3.

Histologic analysis. Hematoxylin/eosin sections of ML006 (**A**), ML017 (**B**), or ML017/ET (**C**) xenografts collected before and 14 days after the end of treatment with trabectedin. The additional picture in **A** was taken from one of the long-lasting regressed cases at the end of the observation period, and shows a diffuse mostly monovacuolated lipoblastic growth in the myxoid matrix.

trabectedin and suggest that restoring adipogenesis may represent a rational strategy to overcome it.

Molecular studies performed in human samples showed that PPARγ is expressed at high levels—comparable with normal fat—in most liposarcoma histotypes but not in other STS subtypes (24). The treatment of primary cultures of liposarcomas obtained from surgically resected sarcomas treated with pioglitazone showed lipid accumulation and morphologic changes characteristic of mature adipocytes. Differentiation was not observed in primary cultures of different STS histotypes that did not express PPARγ. These data suggest that the block of differentiation in liposarcomas as a consequence of different molecular reasons may be overcome by stimulation of PPARγ (23).

Clinical studies report tumor responses after treatment with PPARγ agonists in patients affected by MLS. Demetri and colleagues observed "dramatic histologic changes" in two cases of MLS and one pleomorphic liposarcoma patient treated with troglitazone (29). Posttreatment samples were characterized by lipid accumulation in the cytoplasm and increased cell volume without changes in the morphology of the nuclei. MRI scans performed after 6 weeks of treatment showed a moderate increase in tumor mass with changes in fat density signals compared with pretreatment images. These findings are consistent with those observed in our xenograft models after treatment with pioglitazone as reported here. Histologically, they showed diffuse lipid accumulation in tumor cells exhibiting microvesicular cytoplasm coupled with nuclear footprints of stemness, and rapid growth that was associated with an initial tumor progression. These similarities between clinical and preclinical observations corroborate the potential clinical relevance of our data.

More recently, a prolonged partial response lasting 690 days was observed in a patient with MLS enrolled in the phase I study of

Published OnlineFirst September 3, 2019; DOI: 10.1158/1078-0432.CCR-19-0976

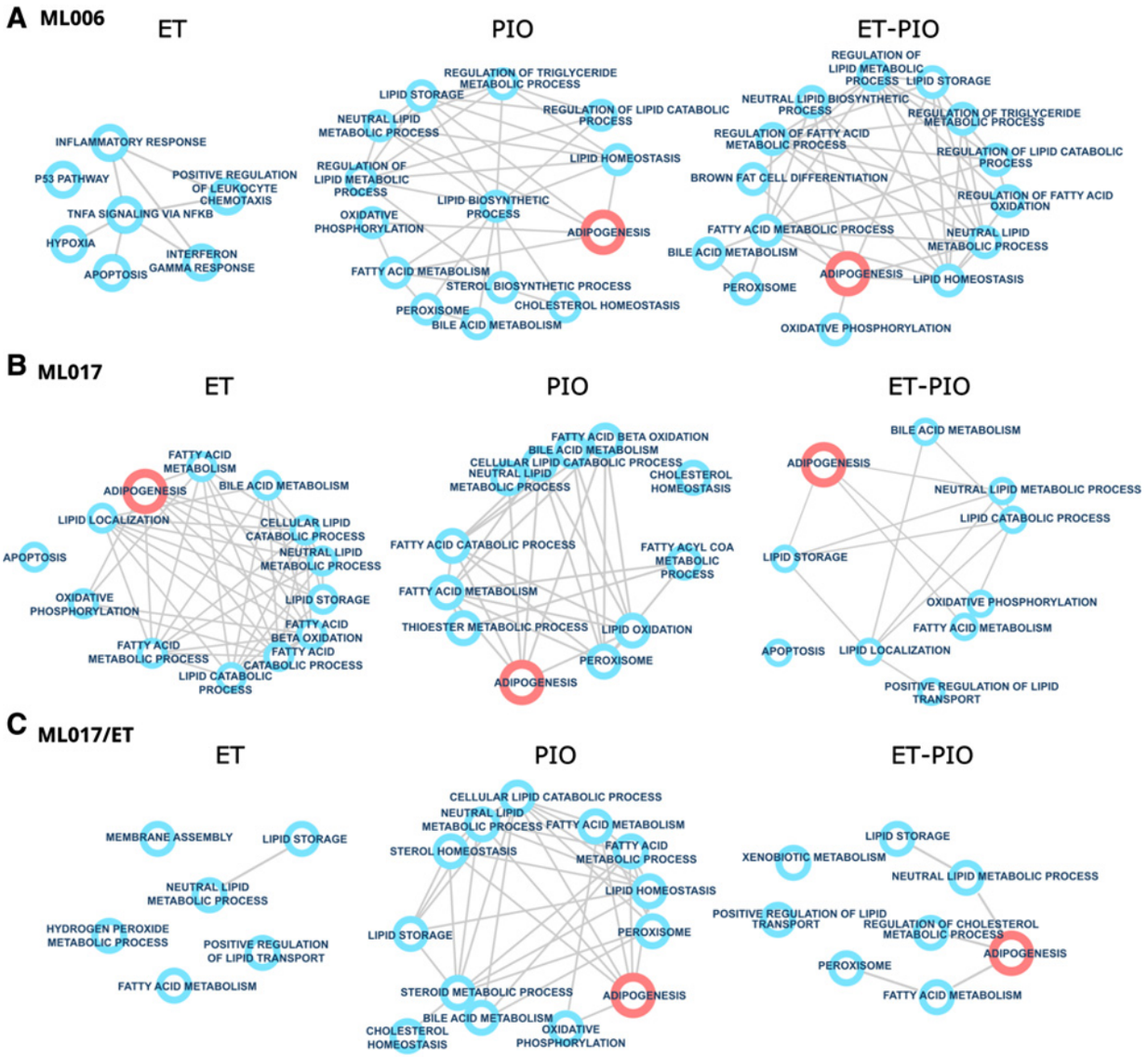

Figure 4.

Biological processes. The figure shows a selection of significant pathways evaluated as reported in Materials and Methods. Each circle refers to a biological process. Adipogenesis process is highlighted in red where present. Edges are built on the presence of genes for each couple of pathway. **A,** ML006; **B,** ML017; **C,** ML017/ET. For each PDX type, results are reported with the following treatment order: trabectedin (ET), pioglitazone (PIO), trabectedin plus pioglitazone (ET-PIO).

efatutazone. Subsequent surgical resection demonstrated the absence of viable disease in three of four remaining neoplastic lesions and the patient remained tumor free at the last reevaluation 3 years after treatment start (31).

Collectively, these data are consistent with the notion that within the myxoid–RC continuum, both trabectedin-sensitive and -resistant RC variants retain the machinery to activate the adipocytic program that may be targeted pharmacologically.

The possibility to combine PPARγ agonists and trabectedin was first proposed by Charytonowicz and colleagues (32). They generated genetically modified mice expressing FUS–CHOP under the control of the mesoderm-specific promoter Prx1 and crossed them with p53-null mice to obtain spontaneous tumor formation. The resultant TCp53-null mice were treated with trabectedin, the PPARγ agonist rosiglitazone, or with the combination of both after the emergence of sarcoma. Trabectedin-treated mice displayed increased survival associated with dramatic adipocytic differentiation and these were even more marked in mice on the combination. Rosiglitazone alone did not affect outcomes compared with untreated mice. Interestingly, all untreated and rosiglitazone-treated mice died of sarcoma progression, whereas mice that received the combination and half of the mice treated with

Published OnlineFirst September 3, 2019; DOI: 10.1158/1078-0432.CCR-19-0976

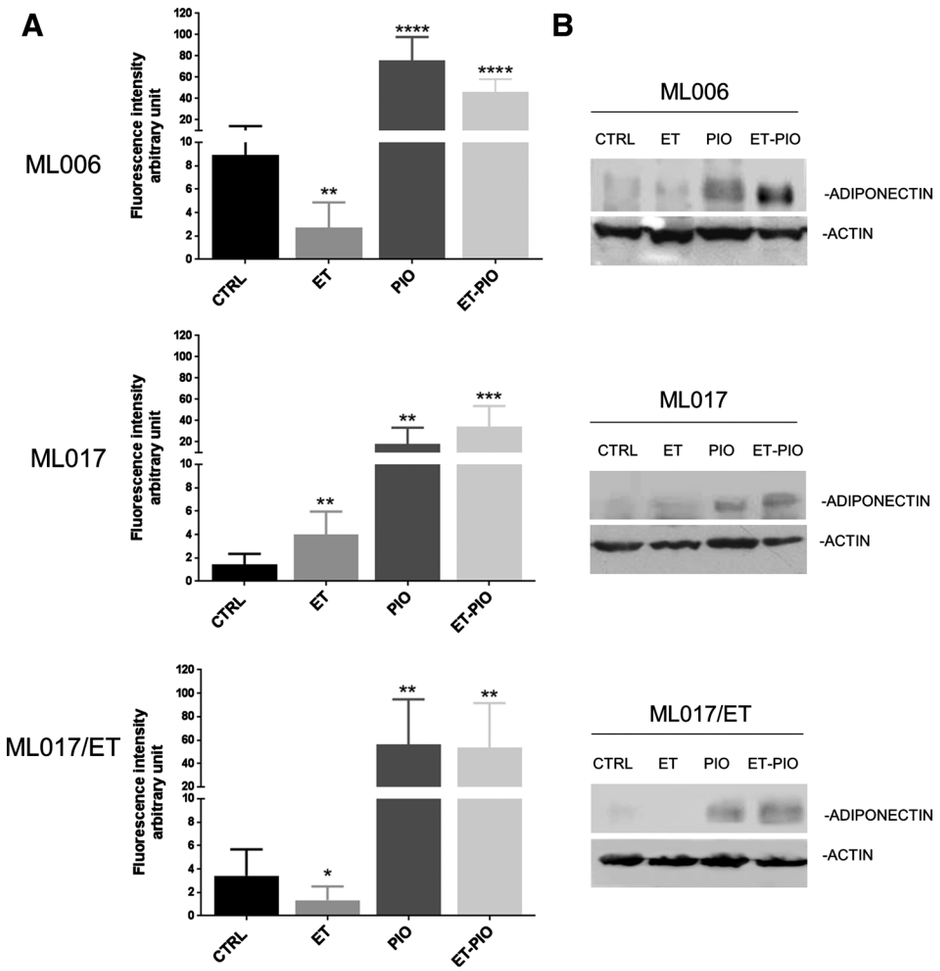

Figure 5.
Validation of *ADIPOQ* as a marker of adipogenesis. Bar graphs show expression levels of *ADIPOQ* before and after treatments (**A**). ET, trabectedin; PIO, pioglitazone; ET-PIO trabectedin plus pioglitazone. Data show that *ADIPOQ* is upregulated (*, $P < 0.05$; **, $P < 0.01$; ***, $P < 0.001$; ****, $P < 0.0001$) where adipogenesis is a significant biological process (Fig. 4). All these results were further confirmed by Western blot (**B**).

trabectedin died of secondary lymphoma related to the loss of p53. This observation suggests that the combination of trabectedin and PPARγ agonist may not only improve trabectedin efficacy but may eventually lead to the cure of the original sarcoma.

In our work, we demonstrated that the combination of trabectedin and pioglitazone can increase the efficacy of trabectedin alone not only in MLS with acquired resistance after many courses of trabectedin treatment, but also in *ab initio*–resistant liposarcomas. Notably, we observed in ML006 tumors with innate resistance against the drug complete regressions in three of nine mice and partial responses, with minimal residual disease, in four of nine mice. At the end of the observation period, tumor regrowth was observed in only one mouse.

Notably, pioglitazone itself did not elicit toxicity, and the toxicity of trabectedin in terms of weight loss was not increased when combined with pioglitazone.

The preclinical findings reported here as well as some previous preclinical and clinical observations reported in the literature provide a strong rationale to undertake a clinical study aimed at assessing if treatment with a PPARγ agonist—such as pioglitazone—increases the efficacy of trabectedin in patients with MLS, leading possibly to a clinically significant prolongation of PFS or even to the cures in some patients. We surmise that the rationale for a clinical study on the combination of PPARγ agonists with trabectedin in MLS is compelling. Yet, there is no evidence that this is also the case for other liposarcomas, even though it is known that all liposarcomas express high levels of PPARγ receptors. This issue is currently under preclinical evaluation using appropriate preclinical models of liposarcomas other than MLS.

One aspect that needs to be considered in the design of a clinical study of the combination of a PPARγ agonist with trabectedin is that in our preclinical models the efficacy of pioglitazone became evident only after prolonged chronic treatment lasting several weeks. Designers of clinical trials who aim at testing this combination should bear the requirement of prolonged treatment with the PPARγ agonist in mind.

Therefore, the efficacy of coadministration of trabectedin with pioglitazone should be explored early on during treatment, when tumor growth is still controlled by trabectedin, definitely before the tumor has acquired robust resistance against trabectedin leading to its rapid progression.

Disclosure of Potential Conflicts of Interest

P.G. Casali reports receiving speakers bureau honoraria from PharmaMar, Eisai, Pfizer and Eli Lilly, and is a consultant/advisory board member for Bayer, Deciphera, Eisai, and Nektar Pharm. A. Gronchi reports receiving speakers bureau honoraria from Novartis, Pfizer, Bayer, Lilly, PharmaMar, Nanobiotix and SpringWorks, and reports receiving commercial research grants from PharmaMar. No potential conflicts of interest were disclosed by the other authors.

Authors' Contributions

Conception and design: R. Frapolli, A. Gronchi, S. Pilotti, M. D'Incalci
Development of methodology: R. Frapolli, E. Bello, P. Ubezio, L. Porcu
Acquisition of data (provided animals, acquired and managed patients, provided facilities, etc.): R. Frapolli, E. Bello, M. Ponzo, I. Craparotta, S. Ballabio, L. Carrassa, S. Brich, R. Sanfilippo, P.G. Casali, A. Gronchi, S. Pilotti
Analysis and interpretation of data (e.g., statistical analysis, biostatistics, computational analysis): R. Frapolli, L. Mannarino, S. Marchini, L. Carrassa, P. Ubezio, L. Porcu, R. Sanfilippo, P.G. Casali, S. Pilotti
Writing, review, and/or revision of the manuscript: R. Frapolli, E. Bello, L. Mannarino, P. Ubezio, L. Porcu, R. Sanfilippo, A. Gronchi, S. Pilotti, M. D'Incalci
Study supervision: R. Frapolli, S. Pilotti, M. D'Incalci

Acknowledgments

This work was supported by the Italian Association for Cancer Research grant to M. D'Incalci (Project Number 19189).

The costs of publication of this article were defrayed in part by the payment of page charges. This article must therefore be hereby marked *advertisement* in accordance with 18 U.S.C. Section 1734 solely to indicate this fact.

Received March 28, 2019; revised July 1, 2019; accepted August 28, 2019; published first September 3, 2019.

References

1. D'Incalci M, Galmarini CM. A review of trabectedin (ET-743): a unique mechanism of action. Mol Cancer Ther 2010;9:2157–63.
2. D'Incalci M, Badri N, Galmarini CM, Allavena P. Trabectedin, a drug acting on both cancer cells and the tumour microenvironment. Br J Cancer 2014; 111:646–50.
3. Larsen AK, Galmarini CM, D'Incalci M. Unique features of trabectedin mechanism of action. Cancer Chemother Pharmacol 2016;77:663–71.
4. Yondelis | European Medicines Agency [Internet]. [cited 2018 Oct 12]. Available from: https://www.ema.europa.eu/en/medicines/human/EPAR/yondelis
5. Barone A, Chi D-C, Theoret MR, Chen H, He K, Kufrin D, et al. FDA approval summary: trabectedin for unresectable or metastatic liposarcoma or leiomyosarcoma following an anthracycline-containing regimen. Clin Cancer Res 2017;23:7448–53.
6. Grosso F, Jones RL, Demetri GD, Judson IR, Blay J-Y, Le Cesne A, et al. Efficacy of trabectedin (ecteinascidin-743) in advanced pretreated myxoid liposarcomas: a retrospective study. Lancet Oncol 2007;8:595–602.
7. Grosso F, Sanfilippo R, Virdis E, Piovesan C, Collini P, Dileo P, et al. Trabectedin in myxoid liposarcomas (MLS): a long-term analysis of a single-institution series. Ann Oncol 2009;20:1439–44.
8. Gronchi A, Bui BN, Bonvalot S, Pilotti S, Ferrari S, Hohenberger P, et al. Phase II clinical trial of neoadjuvant trabectedin in patients with advanced localized myxoid liposarcoma. Ann Oncol 2012;23:771–6.
9. Gronchi A, Ferrari S, Quagliuolo V, Broto JM, Pousa AL, Grignani G, et al. Histotype-tailored neoadjuvant chemotherapy versus standard chemotherapy in patients with high-risk soft-tissue sarcomas (ISG-STS 1001): an international, open-label, randomised, controlled, phase 3, multicentre trial. Lancet Oncol 2017;18:812–22.
10. Saponara M, Stacchiotti S, Gronchi A. The safety and efficacy of trabectedin for the treatment of liposarcoma or leiomyosarcoma. Expert Rev Anticancer Ther 2016;16:473–84.
11. Kuroda M, Ishida T, Takanashi M, Satoh M, Machinami R, Watanabe T. Oncogenic transformation and inhibition of adipocytic conversion of preadipocytes by TLS/FUS-CHOP type II chimeric protein. Am J Pathol 1997;151:735–44.
12. Pérez-Losada J, Pintado B, Gutiérrez-Adán A, Flores T, Bañares-González B, Calabia del Campo J, et al. The chimeric FUS/TLS-CHOP fusion protein specifically induces liposarcomas in transgenic mice. Oncogene 2000;19: 2413–22.
13. Pérez-Losada J, Sánchez-Martín M, Rodríguez-García MA, Pérez-Mancera PA, Pintado B, Flores T, et al. Liposarcoma initiated by FUS/TLS-CHOP: the FUS/TLS domain plays a critical role in the pathogenesis of liposarcoma. Oncogene 2000;19:6015–22.
14. Engström K, Willén H, Kåbjörn-Gustafsson C, Andersson C, Olsson M, Göransson M, et al. The myxoid/round cell liposarcoma fusion oncogene FUS-DDIT3 and the normal DDIT3 induce a liposarcoma phenotype in transfected human fibrosarcoma cells. Am J Pathol 2006;168:1642–53.
15. Riggi N, Cironi L, Provero P, Suvà M-L, Stehle J-C, Baumer K, et al. Expression of the FUS-CHOP fusion protein in primary mesenchymal progenitor cells gives rise to a model of myxoid liposarcoma. Cancer Res 2006;66:7016–23.
16. Pérez-Mancera PA, Bermejo-Rodríguez C, Sánchez-Martín M, Abollo-Jiménez F, Pintado B, Sánchez-García I. FUS-DDIT3 prevents the development of adipocytic precursors in liposarcoma by repressing PPARγ and C/EBPα and activating eIF4E. PLoS ONE 2008;3:e2569.
17. Rodriguez R, Tornin J, Suarez C, Astudillo A, Rubio R, Yauk C, et al. Expression of FUS-CHOP fusion protein in immortalized/transformed human mesenchymal stem cells drives mixoid liposarcoma formation. Stem Cells 2013;31:2061–72.
18. Frapolli R, Tamborini E, Virdis E, Bello E, Tarantino E, Marchini S, et al. Novel models of myxoid liposarcoma xenografts mimicking the biological and pharmacologic features of human tumors. Clin Cancer Res 2010;16: 4958–67.
19. Di Giandomenico S, Frapolli R, Bello E, Uboldi S, Licandro SA, Marchini S, et al. Mode of action of trabectedin in myxoid liposarcomas. Oncogene 2014;33:5201–10.
20. Bello E, Brich S, Craparotta I, Mannarino L, Ballabio S, Gatta R, et al. Establishment and characterisation of a new patient-derived model of myxoid liposarcoma with acquired resistance to trabectedin. Br J Cancer 2019;121:464–73.
21. Lowe CE, O'Rahilly S, Rochford JJ. Adipogenesis at a glance. J Cell Sci 2011; 124:2681–6.
22. Sato H, Ishihara S, Kawashima K, Moriyama N, Suetsugu H, Kazumori H, et al. Expression of peroxisome proliferator-activated receptor (PPAR)γ in gastric cancer and inhibitory effects of PPARγ agonists. Br J Cancer 2000;83: 1394–400.
23. Takashima T, Fujiwara Y, Higuchi K, Arakawa T, Yano Y, Hasuma T, et al. PPAR-γ ligands inhibit growth of human esophageal adenocarcinoma cells through induction of apoptosis, cell cycle arrest and reduction of ornithine decarboxylase activity. Int J Oncol 2001;19:465–71.
24. Tontonoz P, Hu E, Spiegelman BM. Stimulation of adipogenesis in fibroblasts by PPARγ2, a lipid-activated transcription factor. Cell 1994; 79:1147–56.
25. Tontonoz P, Singer S, Forman BM, Sarraf P, Fletcher JA, Fletcher CDM, et al. Terminal differentiation of human liposarcoma cells induced by ligands for peroxisome proliferator-activated receptor γ and the retinoid X receptor. Proc Natl Acad Sci U S A 1997;94:237–41.
26. Lu M, Kwan T, Yu C, Chen F, Freedman B, Schafer JM, et al. Peroxisome proliferator-activated receptor gamma agonists promote TRAIL-induced apoptosis by reducing survivin levels via cyclin D3 repression and cell cycle arrest. J Biol Chem 2005;280:6742–51.
27. Kulke MH, Demetri GD, Sharpless NE, Ryan DP, Shivdasani R, Clark JS, et al. A phase II study of troglitazone, an activator of the PPARgamma receptor, in patients with chemotherapy-resistant metastatic colorectal cancer. Cancer J Sudbury Mass 2002;8:395–9.
28. Burstein HJ, Demetri GD, Mueller E, Sarraf P, Spiegelman BM, Winer EP. Use of the peroxisome proliferator-activated receptor (PPAR) gamma ligand troglitazone as treatment for refractory breast cancer: a phase II study. Breast Cancer Res Treat 2003;79:391–7.
29. Debrock G, Vanhentenrijk V, Sciot R, Debiec-Rychter M, Oyen R, Van Oosterom A. A phase II trial with rosiglitazone in liposarcoma patients. Br J Cancer 2003;89:1409–12.
30. Demetri GD, Fletcher CDM, Mueller E, Sarraf P, Naujoks R, Campbell N, et al. Induction of solid tumor differentiation by the peroxisome proliferator-activated receptor-γ ligand troglitazone in patients with liposarcoma. Proc Natl Acad Sci U S A 1999;96:3951–6.

Published OnlineFirst September 3, 2019; DOI: 10.1158/1078-0432.CCR-19-0976

31. Pishvaian MJ, Marshall JL, Wagner AJ, Hwang JJ, Malik S, Cotarla I, et al. A phase 1 study of efatutazone, an oral peroxisome proliferator-activated receptor gamma agonist, administered to patients with advanced malignancies. Cancer 2012;118:5403–13.
32. Charytonowicz E, Terry M, Coakley K, Telis L, Remotti F, Cordon-Cardo C, et al. PPARγ agonists enhance ET-743–induced adipogenic differentiation in a transgenic mouse model of myxoid round cell liposarcoma. J Clin Invest 2012;122:886–98.
33. Workman P, Aboagye EO, Balkwill F, Balmain A, Bruder G, Chaplin DJ, et al. Guidelines for the welfare and use of animals in cancer research. Br J Cancer 2010;102:1555–77.
34. Discovery & Development Services | DTP [Internet]. [cited 2019 Mar 20]. Available from: https://dtp.cancer.gov/discovery_development/nci-60/methodology.htm.
35. Shoemaker RH. The NCI60 human tumour cell line anticancer drug screen. Nat Rev Cancer 2006;6:813–23.
36. Vázquez R, Licandro SA, AstorguesXerri L, Lettera E, Panini N, Romano M, et al. Promising in vivo efficacy of the BET bromodomain inhibitor OTX015/MK-8628 in malignant pleural mesothelioma xenografts. Int J Cancer 2017;140:197–207.
37. Bizzaro F, Falcetta F, D'Agostini E, Decio A, Minoli L, Erba E, et al. Tumor progression and metastatic dissemination in ovarian cancer after dose-dense or conventional paclitaxel and cisplatin plus bevacizumab. Int J Cancer 2018;143:2187–99.
38. Fletcher CDM. The evolving classification of soft tissue tumours – an update based on the new 2013 WHO classification. Histopathology 2014;64:2–11.
39. Calura E, Martini P, Sales G, Beltrame L, Chiorino G, D'Incalci M, et al. Wiring miRNAs to pathways: a topological approach to integrate miRNA and mRNA expression profiles. Nucleic Acids Res 2014;42:e96.
40. Bolstad BM, Irizarry RA, Astrand M, Speed TP. A comparison of normalization methods for high density oligonucleotide array data based on variance and bias. Bioinforma Oxf Engl 2003;19:185–93.
41. Smyth GK, Ritchie M, Thorne N, Wettenhall J, Shi W, Hu Y. limma: linear models for microarray and RNA-seq data. User's guide. 2002.
42. Leek J, Johnson W, Parker H, Fertig E, Jaffe A, Storey J, et al. sva [Internet]. Bioconductor. 2018 [cited 2019 Mar 15]. Available from: http://bioconductor.org/packages/sva/
43. Benjamini Y, Drai D, Elmer G, Kafkafi N, Golani I. Controlling the false discovery rate in behavior genetics research. Behav Brain Res 2001;125:279–84.
44. Subramanian A, Tamayo P, Mootha VK, Mukherjee S, Ebert BL, Gillette MA, et al. Gene set enrichment analysis: a knowledge-based approach for interpreting genome-wide expression profiles. Proc Natl Acad Sci U S A 2005;102:15545–50.
45. Liberzon A, Birger C, Thorvaldsdóttir H, Ghandi M, Mesirov JP, Tamayo P. The Molecular Signatures Database (MSigDB) hallmark gene set collection. Cell Syst 2015;1:417–25.
46. Ashburner M, Ball CA, Blake JA, Botstein D, Butler H, Cherry JM, et al. Gene Ontology: tool for the unification of biology. Nat Genet 2000;25:25–9.
47. Carrassa L, Sanchez Y, Erba E, Damia G. U2OS cells lacking Chk1 undergo aberrant mitosis and fail to activate the spindle checkpoint. J Cell Mol Med 2009;13:1565–76.
48. Chikka MR, McCabe DD, Tyra HM, Rutkowski DT. C/EBP homologous protein (CHOP) contributes to suppression of metabolic genes during endoplasmic reticulum stress in the liver. J Biol Chem 2013;288:4405–15.
49. Rutkowski DT, Wu J, Back S-H, Callaghan MU, Ferris SP, Iqbal J, et al. UPR pathways combine to prevent hepatic steatosis caused by ER stress-mediated suppression of transcriptional master regulators. Dev Cell 2008;15:829–40.
50. Forni C, Minuzzo M, Virdis E, Tamborini E, Simone M, Tavecchio M, et al. Trabectedin (ET-743) promotes differentiation in myxoid liposarcoma tumors. Mol Cancer Ther 2009;8:449–57.

Correction: Combination of PPARγ Agonist Pioglitazone and Trabectedin Induce Adipocyte Differentiation to Overcome Trabectedin Resistance in Myxoid Liposarcomas

Roberta Frapolli, Ezia Bello, Marianna Ponzo, Ilaria Craparotta, Laura Mannarino, Sara Ballabio, Sergio Marchini, Laura Carrassa, Paolo Ubezio, Luca Porcu, Silvia Brich, Roberta Sanfilippo, Paolo Giovanni Casali, Alessandro Gronchi, Silvana Pilotti, and Maurizio D'Incalci

In the original version of this article (1), the accession number was incorrect. The error has been corrected in the latest online HTML and PDF versions of the article. The authors regret this error.

Reference

1. Frapolli R, Bello E, Ponzo M, Craparotta I, Mannarino L, Ballabio S, et al. Combination of PPARγ agonist pioglitazone and trabectedin induce adipocyte differentiation to overcome trabectedin resistance in myxoid liposarcomas. Clin Cancer Res 2019;25:7565–75.

Published online March 2, 2020.
Clin Cancer Res 2020;26:1199
doi: 10.1158/1078-0432.CCR-20-0172

Published OnlineFirst September 3, 2019; DOI: 10.1158/1078-0432.CCR-19-0976

Clinical Cancer Research

Combination of PPARγ Agonist Pioglitazone and Trabectedin Induce Adipocyte Differentiation to Overcome Trabectedin Resistance in Myxoid Liposarcomas

Roberta Frapolli, Ezia Bello, Marianna Ponzo, et al.

Clin Cancer Res 2019;25:7565-7575. Published OnlineFirst September 3, 2019.